J. Appl. Comput. Mech., 5(4) (2019) 667-679
DOI: 10.22055/JACM.2019.27058.1372

ISSN: 2383-4536
jacm.scu.ac.ir

M&MoCS

Shahid Chamran University of Ahvaz

Journal of Applied and Computational Mechanics

Research Paper

Elastic Behavior of Functionally Graded Two Tangled Circles Chamber

Javad Jafari Fesharaki, Mehran Roghani

Department of Mechanical Engineering, Najafabad Branch, Islamic Azad University, Najafabad, 8514143131, Iran

Received September 11 2018; Revised December 31 2018; Accepted for publication January 05 2019.
Corresponding author: Javad Jafari Fesharaki, Jafari@pmc.iaun.ac.ir

Abstract. This paper presents the numerical elastic solution for a real problem, functionally graded chamber of hydraulic gear pumps under internal pressure. Because of the similarity and complexity for the considering geometry, a bipolar cylindrical coordinate system is used to extract the governing equations. The material properties are considered to vary along the two tangled circles with a power-law function. The two coupled governing equations solved by the differential quadrature method. The results are presented for various material index and show that the complexity in considering geometry and material inhomogeneity can change the stress and displacements value through the geometry efficiently. The results and presented method in this paper for extracting and solving the problem can be used for designing similar geometry more accurate. The results of this research are compared with those reported in the previous work.

Keywords: Complex geometry, Bipolar cylindrical coordinate, Functionally graded material, Differential quadrature method, Two tangled circles chamber.

1. Introduction

In the past few years, a new kind of in-homogeneous composite materials named functionally graded materials (FGMs) has attracted the considerable attention of many material scientists and engineers, mainly because recent developments of nano/micro-technologies are allowing us to design their microstructures. FGMs are mainly constructed of two different materials (e.g. ceramic and metal) and have a smooth and continuous variation of their physical properties along the desired direction in geometry. This continuous variation prevents stress concentrations near geometric and material discontinuities, and it can have the advantages of both materials like high-temperature resistance of ceramics and ductility and high load bearing of metals. On the other hand, the differential quadrature method (DQM) is a recent numerical method that provides an accurate and efficient solution of partial differential equations by approximating the partial derivative of a function to a weighted summation of that function at intermediate points.

Using differential quadrature along with discrete singular convolution Ersoy et al. [1] analyzed free vibration of curved structural components for FGM and laminated shells. Beni and Dehkordi [2] utilized generalized differential quadrature and the Carrera unified formulation to study circular sandwich plates with FGM core. Wang and Yuan [3] presented a two-dimensional elasticity analysis on sandwich panels using DQM. Hosseini et al. [4] analyzed the effects of strain gradient on the thermoelastic response of micro-rotating FGM cylinder using generalize differential quadrature method. By using the three-dimensional theory of elasticity Demirbas presented thermal stress analyzes of FGM plates that have temperature-dependent physical properties[5]. Mehditabar et al. [6] studied FGM cylindrical shells with a three-dimensional thermo-magneto-elastic analysis using DQM. Brischetto et al. [7] obtained the exact three-dimensional solution for analyzing free vibration of FGM cylinders and plates. They also proposed several 2D numerical solutions including refined and classic generalized differential quadrature and finite elements. Parand and Alibeigloo [8] presented a vibration and static analysis of cylindrical sandwich shells with FGM core. They used Fourier series expansion to analytically solve cylindrical sandwich shells with simply supported boundary conditions and differential quadrature for the numerical solution of other boundary conditions. Adineh and Kadkhodayan [9] carried out a 3D dynamic response and thermo-elastic analysis of a functionally graded multidirectional skew plate using differential quadrature method. Fesharaki et al. [10] obtained a 2D exact solution for the electro-mechanical behavior of FGM piezoelectric hollow cylinder using complex Fourier series. Eringen's nonlocal theory of elasticity and the modified couple stress theory are utilized to study the nonlinear thermal buckling of FGM micro/nanobeams by Shafiei et al. [11]. Zghal et al. worked on vibration and buckling of functionally graded carbon nanotubes-reinforced composite plate [12, 13]. Yang et al. [14] investigated the buckling and post-buckling of FGM composite beams reinforced with graphene platelets using differential quadrature method. Daviran et al. [15] performed a thermal shock analysis on metal-ceramic FGM discs reinforced with carbon nanotubes using DQM. Based on von Karman hypothesis and Mindlin's strain gradient elasticity theory Ansari et al. [16] investigated the mechanical behavior of FGM third-order shear deformable microbeams. They used variational differential quadrature method along with the pseudo arc-length continuation method and periodic time differential operators to achieve the numerical solution to their problem. Atrian et al. [17] derived the analytical solution of the thermo-electromechanical response of piezoelectric FGM hollow cylinder subjected to non-axisymmetric loads. Bahadori and Najafizadeh [18] adopted a generalized differential quadrature method and first-order shear deformation theory in order to investigate free vibration of 2D FGM cylindrical shells resting on Winkler-Pasternak elastic foundation. Ansari et al. [19] analyzed 3D vibrational and bending of FGM nanoplates by variational differential quadrature method. Zghal et al worked on FGM carbon nanotube-reinforced shells under static and dynamic loads [20, 21]. They investigated the effects of length-to-thickness ratio, carbon nanotube volume fraction, geometrical parameters and boundary conditions on the behavior of shell structures. Alibeigloo and Nouri [22] presented a 3D solution static analysis of piezoelectric FGM cylindrical shells using a state-space approach and DQM. Thermo-mechanical bending analysis of FGM sandwich plates was carried out by Li et al. [23]. They used four-variable refined plate theory along with Navier approach to derive and solve the governing equations. Norouzi and Alibeigloo [24] investigated the 3D static of functionally graded viscoelastic cylindrical panels using state-space DQM. Using Hamilton's principle and transverse shear deformation theory for the equation of motion and discrete singular convolution method to obtain the eigenvalue problem of the system Civalek investigated free vibration of cylindrical and conical shells and annular plates made of FGM and composite laminated materials [25]. Alashti and Khorsand [26] carried out a 3D elastic analysis of FGM piezoelectric cylindrical shells subjected to thermal and dynamic loads based on a coupled DQ-FD method. Using the finite element method, Zghal et al. worked on bending analysis of composites reinforced by graphene-nanotubes [27]. Frikha et al. worked on functionally graded carbon nanotubes-reinforced composites [28]. Yas and Aragh [29] presented the 3D elasticity solution for free vibration analysis of cylindrical panels made of a 4-parameter functionally graded fiber orientation composite. Using the standard DQM operators Shojaei and Ansari [30] directly discretized the energy functional in structural mechanics to develop a new solution method to simplify numerical structures analysis named variational differential quadrature. Setoodeh et al. [31] employed the layerwise theory and differential quadrature method to analyze the transient dynamic behavior of cylindrical FGM shells under dynamic pressure. Malekzadeh [32] studied the 3D thermal buckling of FGM quadrilateral plates that are arbitrary straight sided with DQM. Jodaei et al. [33] analyzed the free vibration of FGM annular plates. They used a differential quadrature method that is state-space based to obtain the frequencies of vibration and an artificial neural network comparative behavior modeling for various boundary conditions. Using Timoshenko beam theory and DQM Janghorban and Zare [34] investigated free vibration of FGM carbon nanotubes with varied thickness. Alibeigloo and Liew [35] presented the elasticity solution of bending behavior and vibration of composite beam reinforced with functionally graded carbon nanotubes with piezoelectric layers using DQM. Trabelsi et al. used first-order shear deformation theory to investigate the thermal buckling and post-buckling of functionally graded plated and cylindrical shells [36, 37]. Based on the elasticity theory Heidarpour et al. [38] investigated the thermoelastic behavior of rotating cylindrical shells made of laminated FGM using layerwise DQM. Alashti and Khorsand [39] analyzed the 3D thermoelastic behavior of FGM piezoelectric cylindrical shells. They used Fourier and polynomial quadrature methods in order to obtain the results in thermal, displacement and stress fields.

In this paper, a functionally graded geometry like a hydraulic pump chamber is investigated. The shape of the chamber is considered like two tangled circles. To extract the governing equations and boundary conditions, because of complexity in geometry, the bipolar cylindrical coordinate is considered. The material properties are varied along the chamber thickness except for the Poisson's ratio. The two coupled governing equations solved by the differential quadrature method.

2. Problem Definition

Consider a thick functionally graded hollow cylinder with two tangled circles. The considering problem is like a hydraulic gear pumps chamber. Because of complexity in considering geometry, a bipolar cylindrical coordinate system is considered for extracting the equations. The coordinate and considering problem is shown in Fig. 1.

According to considering special geometry for the problem (two tangled circles hole), the formulation presented in two directions. Considering that, "u" and "v" to be the displacements along the two tangled circles and two separate circles direction along "ξ" and "h" direction respectively. Thus, in the bipolar cylinderical coordinate system, the relation between displacements and strains along the tangled circles and separate circles directions presents (from Appendix A):

$$\varepsilon_{\xi\xi} = \frac{(\cos\eta - \cos\xi)}{a}\frac{\partial u}{\partial \xi} - \frac{\sinh\eta}{a}v \tag{1a}$$

$$\varepsilon_{\eta\eta} = \frac{-\sin\xi}{a}u + \frac{(\cos\eta - \cos\xi)}{a}\frac{\partial v}{\partial \eta} \tag{1b}$$

$$\varepsilon_{\xi\eta} = \frac{1}{2}\left(\frac{(\cos\eta - \cos\xi)}{a}\frac{\partial u}{\partial \eta} + \frac{(\cos\eta - \cos\xi)}{a}\frac{\partial v}{\partial \xi} - \frac{\sinh\eta}{a}u\right) \tag{1c}$$

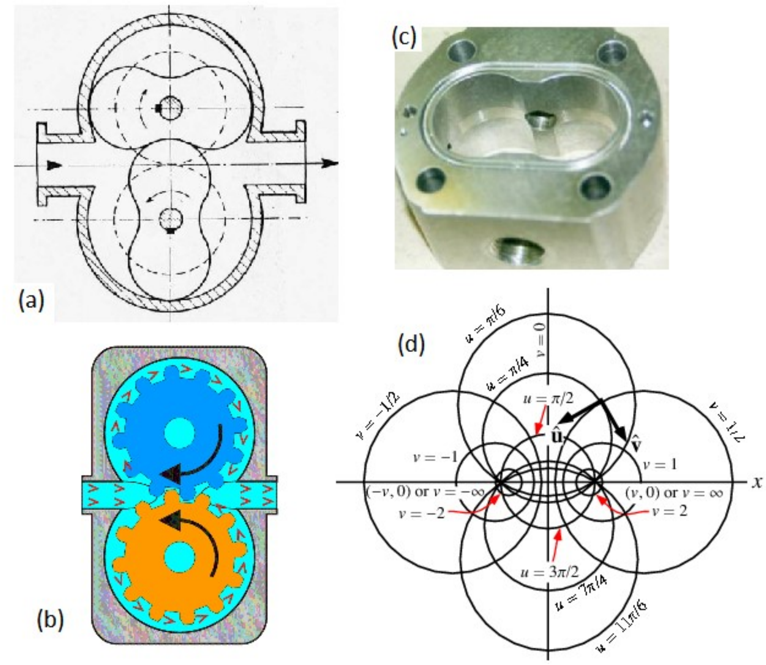

Fig. 1. (a) and (b) schematic of two kinds of hydraulic gear pumps, (c) real hydraulic gear chamber, (d) considering coordinate (Bipolar cylindrical coordinate)

The relation between strain and components for considering geometry can be expressed as:

$$T_{\xi\xi} = N_{11}^{g} \cdot \varepsilon_{\xi\xi} + N_{12}^{g} \cdot \varepsilon_{\eta\eta} \tag{2a}$$

$$T_{\eta\mu} = N_{12}^{g} \cdot \varepsilon_{\xi\xi} + N_{22}^{g} \cdot \varepsilon_{\eta\eta} \tag{2b}$$

$$T_{\xi\eta} = 2N_{12}^{g} \cdot \varepsilon_{\xi\eta} \tag{2c}$$

where the $N_{ij}^{g}(i, j = 1,2,3)$ and $T_{ij}\,(i, j = \xi,\eta)$ are the elastic coefficients and stress tensor component respectively. The superscript "g" is used to show the functionally graded material properties. For considering the functionally graded properties for material, suppose that all material coefficients are graded through the two tangled circles direction "ξ", thus the material properties are functions of "ξ" as:

$$N_{ij}^{g} = N_{ij}\,\xi^{p} \quad (i, j = 1,2,3) \tag{3}$$

where N_{ij} and "p" are the outer surface of cylinder property and power-law index for FGM properties respectively. Also, irrespective of the body force, for a functionally graded cylinder with two tangled circles hole, the equilibrium equations in bipolar the cylindrical coordinate system are expressed as (from Appendix B):

$$\frac{\partial T_{\xi\xi}}{\partial \xi} + \frac{\partial T_{\xi\eta}}{\partial \eta} + \frac{\sin\xi}{(\cosh\eta - \cos\xi)}(T_{\eta\eta} - T_{\xi\xi}) = 0 \tag{4}$$

$$\frac{\partial T_{\eta\eta}}{\partial \eta} + \frac{\partial T_{\xi\eta}}{\partial \xi} - \frac{2\sin\xi}{(\cosh\eta - \cos\xi)}T_{\xi\eta} + \frac{\sinh\eta}{(\cosh\eta - \cos\xi)}(T_{\xi\xi} - T_{\eta\eta}) = 0 \tag{5}$$

Substituting equations (1)-(3) into Eqs. (4) and (5), based on displacement components the two coupled governing differential equations express:

$$\begin{aligned}&\frac{\partial^2 u}{\partial \xi^2}+c_1\frac{\partial^2 u}{\partial \eta^2}+\frac{p}{\xi}\frac{\partial u}{\partial \xi}+c_2\frac{\partial^2 v}{\partial \xi \partial \eta}+c_3\frac{\sinh\eta}{(\cosh\eta-\cos\xi)}\frac{\partial v}{\partial \xi}+c_4\frac{\sin\xi}{(\cosh\eta-\cos\xi)}\frac{\partial v}{\partial \eta}+c_5\frac{p}{\xi}\frac{\partial v}{\partial \eta}\\&+c_6\frac{\sinh\eta}{(\cosh\eta-\cos\xi)}\frac{\partial u}{\partial \eta}+c_5\frac{p}{\xi}\frac{\sin\xi}{(\cosh\eta-\cos\xi)}u+c_5\frac{\cos\xi}{(\cosh\eta-\cos\xi)}u+c_1\frac{\cos\eta}{(\cosh\eta-\cos\xi)}u\\&+c_7\frac{\sinh^2\xi}{(\cosh\eta-\cos\xi)}u+c_8\frac{p}{\xi}\frac{\sinh\eta}{(\cosh\eta-\cos\xi)}v+c_9\frac{\sin\xi\sinh\eta}{(\cosh\eta-\cos\xi)^2}v=0\end{aligned}\tag{6}$$

$$\begin{aligned}&\frac{\partial^2 v}{\partial \eta^2}+c_{10}\frac{\partial^2 v}{\partial \xi^2}+c_{11}\frac{\partial^2 u}{\partial \xi \partial \eta}+c_{12}\frac{\sinh\eta}{(\cosh\eta-\cos\xi)}\frac{\partial v}{\partial \eta}+c_{13}\frac{p}{\xi}\frac{\partial v}{\partial \xi}+c_{14}\frac{\sinh\eta}{(\cosh\eta-\cos\xi)}\frac{\partial u}{\partial \xi}\\&+c_{15}\frac{\sin\xi}{(\cosh\eta-\cos\xi)}\frac{\partial u}{\partial \eta}+c_{10}\frac{p}{\xi}\frac{\partial u}{\partial \eta}+c_{16}\frac{\sinh^2\eta}{(\cosh\eta-\cos\xi)^2}v+c_{17}\frac{\sin^2\xi}{(\cosh\eta-\cos\xi)^2}v\\&+c_{17}\frac{\cos\xi}{(\cosh\eta-\cos\xi)}v+c_{18}\frac{\cosh\eta}{(\cosh\eta-\cos\xi)}v+c_{13}\frac{p}{\xi}\frac{\sin\xi}{(\cosh\eta-\cos\xi)}v+c_{19}\frac{\sin\xi\sinh\eta}{(\cosh\eta-\cos\xi)^2}u\\&+c_{13}\frac{p}{\xi}\frac{\sinh\xi}{(\cosh\eta-\cos\xi)}u=0\end{aligned}\tag{7}$$

where the constants c_1 to c_{19} are presented in Appendix C.

To specify the displacements along two tangled circles and separate circles directions, two couple equilibrium equations (6) and (7) should solve simultaneously. Solving the differential equations (6) and (7), need four boundary conditions from all possible boundary conditions at the inner and outer surfaces that present:

$$\begin{cases}u(\xi,\eta)=u_0\\ v(\xi,\eta)=v_0\\ T_{\xi\xi}(\xi,\eta)=T^0_{\xi\xi}\\ T_{\eta\eta}(\xi,\eta)=T^0_{\eta\eta}\\ T_{\xi\eta}(\xi,\eta)=T^0_{\xi\eta}\end{cases}\tag{8}$$

Also, by substituting Eq. (1) into Eq. (2), the values for normal and shear stress in terms of displacements yields:

$$T_{\xi\xi}=N_{11}\xi^p\frac{(\cosh\eta-\cos\xi)}{a}\frac{\partial u}{\partial \xi}-N_{11}\xi^p\frac{\sinh\eta}{a}v-N_{12}\xi^p\frac{\sin\xi}{a}u+N_{12}\xi^p\frac{(\cosh\eta-\cos\xi)}{a}\frac{\partial v}{\partial \eta}\tag{9}$$

$$T_{\eta\eta}=N_{12}\xi^p\frac{(\cosh\eta-\cos\xi)}{a}\frac{\partial u}{\partial \xi}-N_{12}\xi^p\frac{\sinh\eta}{a}v-N_{22}\xi^p\frac{\sin\xi}{a}u+N_{22}\xi^p\frac{(\cosh\eta-\cos\xi)}{a}\frac{\partial v}{\partial \eta}\tag{10}$$

$$T_{\xi\eta}=N_{13}\xi^p\frac{(\cosh\eta-\cos\xi)}{a}\frac{\partial u}{\partial \eta}+N_{13}\xi^p\frac{(\cosh\eta-\cos\xi)}{a}\frac{\partial v}{\partial \xi}+N_{13}\xi^p\frac{\sin\xi}{a}u+N_{13}\xi^p\frac{\sinh\eta}{a}u\tag{11}$$

But solving coupled equations (6) and (7) analytically is very difficult. So a powerful numerical method (differential quadrature method-DQM) used to solve the governing equations (6) and (7).

3. Solution by DQM

Differential quadrature method is adopted to solve the equilibrium equations subjected to the desired boundary conditions. DQM is an efficient and accurate method of solving the partial differential equation that was first proposed by Bellman et al. [40]. Some of the advantages of DQM includes converging the solution accurately with a comparatively small number of discretization points and it is a simple adoption procedure that can easily implement various boundary conditions. This method approximates the partial derivative of a function in respect to coordinate variable at a node by a linear weighted summation of the function values of all nodes in that directions. The nth derivative of a function $U(x)$ can be approximated as follows according to the DQM:

$$\left.\frac{\partial^n U}{\partial x^n}\right|_i = \sum_{k=1}^{N} A_{ik}^{(n)} U(x_k) \tag{12}$$

Equation (12) is the general form of the differential quadrature rule in which $A_{ik}^{(n)}$ are the n^{th} order weighting coefficients in the x-direction and "N" is the number of grid points in the x-direction. The weighting coefficients can be calculated by using various kinds of test functions. In this problem, the polynomial test function is used in the radial direction (ξ) and to satisfy the continuity condition in the circumferential direction (h) harmonic test function is used as follows:

$$f(x) = c_0 + \Sigma_{m=1}^{\frac{N}{2}} (c_k \cos\frac{kx}{L} + d_k \sin\frac{kx}{L}) \tag{13}$$

$$g_m(x) = \frac{M(x)}{(x - x_m)M^{(l)}(x_m)}, \quad \text{k=1, 2, ..., N} \tag{14}$$

$$M(x) = (x - x_1)(x - x_2)...(x - x_N)M^{(l)}(x_i) = \Pi_{m=1, m\neq i}^{N} (x_i - x_m) \tag{15}$$

where $f(x)$ is the harmonic test function and $g_m(x)$ is the polynomial test function. Using the above equations and applying them at N grid points, one can calculate the weighting coefficients for each grid point at the desired direction. Subsequently, the explicit formulations to calculate the weighting coefficients are obtained as [41]:

$$a_{ij}^{\xi} = \frac{1}{x_j - x_i} \Pi_{m=1, m\neq i}^{N} \frac{x_i - x_k}{x_j - x_k}, \quad for\ i \neq j \tag{16}$$

$$a_{ii}^{\xi} = \Sigma_{m=1, m\neq i}^{N} \frac{1}{x_j - x_k} \tag{17}$$

$$b_{ij}^{\xi} = \Sigma_{m=1, m\neq i}^{N} a_{ik}^{\xi} a_{kj}^{\xi}, \quad (i, j = 1, 2, ..., N) \tag{18}$$

$$a_{ij}^{\eta} = \frac{q(x_i)}{2\sin(\frac{x_i - x_j}{2}) q(x_j)}, \quad for\ i \neq j \tag{19}$$

$$a_{ii}^{\eta} = -\Sigma_{j=0, i\neq j}^{N} a_{ij} \tag{20}$$

$$q(x_i) = \Pi_{k=0}^{N} \sin(\frac{x_i - x_k}{2}) \tag{21}$$

$$b_{ij}^{\eta} = \Sigma_{k=1}^{N} a_{ik}^{\eta} a_{kj}^{\eta}, \quad (i, j = 1, 2, ..., N) \tag{22}$$

where $a_{ij}^{\xi}, b_{ij}^{\xi}, a_{ij}^{\eta}$ and b_{ij}^{η} denote the weighting coefficients of the first- and second-order derivatives in the x-direction and first- and second-order derivatives in h direction, respectively. Therefore, with the above weighting coefficients that are in one dimension, the approximation can be extended to two-dimensional formulation with the first and second order derivatives defined by:

$$\left.\frac{\partial f}{\partial \xi}\right|_{ij} = \Sigma_{l=1}^{N} a_{il}^{\xi} f_{lj}, \left.\frac{\partial f}{\partial \eta}\right|_{ij} = \Sigma_{m=1}^{N} a_{jm}^{\eta} f_{im} \tag{23}$$

$$\left.\frac{\partial^2 f}{\partial \xi^2}\right|_{ij} = \Sigma_{n=1}^{N} b_{in}^{\xi} f_{nj}, \left.\frac{\partial^2 f}{\partial \eta^2}\right|_{ij} = \Sigma_{k=1}^{N} b_{jk}^{\eta} f_{ik}, \left.\frac{\partial^2 f}{\partial \xi \partial \eta}\right|_{ij} = \Sigma_{n=1}^{N} \Sigma_{k=1}^{N} a_{jn}^{\eta} a_{ik}^{\xi} f_{nk} \tag{24}$$

By implementing equations (12) to (24) into equations (6) and (7) the differential quadrature approximation of the equilibrium equations and stresses yield as:

$$\begin{aligned}&\sum_{n=1}^{N} b_{in}^{\xi} U_{nj} + \frac{p}{\xi}\sum_{l=1}^{N} a_{il}^{\xi} U_{lj} + c_1 \sum_{k=1}^{N} b_{jk}^{\eta} U_{ik} + c_2 \sum_{n=1}^{N}\sum_{k=1}^{N} a_{jn}^{\eta} a_{ik}^{\xi} V_{nk} + c_3 \frac{\sinh\eta}{\cosh\eta-\cos\xi}\sum_{l=1}^{N} a_{il}^{\xi} V_{lj} \\ &+c_4 \frac{\sin\xi}{\cosh\eta-\cos\xi}\sum_{m=1}^{N} a_{jm}^{\eta} V_{im} + c_5 \frac{p}{\xi}\sum_{m=1}^{N} a_{jm}^{\eta} V_{im} + c_6 \frac{\sinh\eta}{\cosh\eta-\cos\xi}\sum_{m=1}^{N} a_{jm}^{\eta} U_{im} \\ &+c_5 \frac{p}{\xi}\frac{\sin\xi}{\cosh\eta-\cos\xi} U + c_5 \frac{\cos\xi}{\cosh\eta-\cos\xi} U + c_1 \frac{\cosh\eta}{\cosh\eta-\cos\xi} U + c_7 \frac{\sinh^2\xi}{(\cosh\eta-\cos\xi)^2} U \\ &+c_8 \frac{p}{\xi}\frac{\sinh\eta}{\cosh\eta-\cos\xi} V + c_9 \frac{\sin\xi\sinh\eta}{(\cosh\eta-\cos\xi)^2} V = 0\end{aligned} \tag{25}$$

$$\begin{aligned}&\sum_{k=1}^{N} b_{jk}^{\eta} V_{ik} + c_{10} \sum_{n=1}^{N} b_{in}^{\xi} V_{nj} + c_{11} \sum_{n=1}^{N}\sum_{k=1}^{N} a_{jn}^{\eta} a_{ik}^{\xi} U_{nk} + c_{12} \frac{\sinh\eta}{\cosh\eta-\cos\xi}\sum_{m=1}^{N} a_{jm}^{\eta} V_{im} + c_{13} \frac{p}{\xi}\sum_{l=1}^{N} a_{il}^{\xi} V_{lj} \\ &+c_{14} \frac{\sinh\eta}{\cosh\eta-\cos\xi}\sum_{l=1}^{N} a_{il}^{\xi} U_{lj} + c_{15} \frac{\sin\xi}{\cosh\eta-\cos\xi}\sum_{m=1}^{N} a_{jm}^{\eta} U_{im} + c_{10} \frac{p}{\xi}\sum_{m=1}^{N} a_{jm}^{\eta} U_{im} \\ &+c_{16} \frac{\sinh^2\eta}{(\cosh\eta-\cos\xi)^2} V + c_{17} \frac{\sin^2\eta}{(\cosh\eta-\cos\xi)^2} V + c_{17} \frac{\cos\xi}{\cosh\eta-\cos\xi} V + c_{18} \frac{\cosh\eta}{\cosh\eta-\cos\xi} V \\ &+c_{13} \frac{p}{\xi}\frac{\sin\xi}{\cosh\eta-\cos\xi} V + c_{19} \frac{\sin\xi\sinh\eta}{(\cosh\eta-\cos\xi)^2} U + c_{13} \frac{p}{\xi}\frac{\sinh\eta}{\cosh\eta-\cos\xi} U = 0\end{aligned} \tag{26}$$

$$T_{\xi\xi} = N_{11}\xi^p A\sum_{l=1}^{N} a_{il}^{\xi} U_{lj} - N_{11}\xi^p \frac{\sinh\eta}{\cosh\eta-\cos\xi} V - N_{12}\xi^p \frac{\sin\xi}{\cosh\eta-\cos\xi} U + N_{12}\xi^p A\sum_{m=1}^{N} a_{jm}^{\eta} V_{im} \tag{27}$$

$$T_{\eta\eta} = N_{12}\xi^p A\sum_{l=1}^{N} a_{il}^{\xi} U_{lj} - N_{12}\xi^p \frac{\sinh\eta}{\cosh\eta-\cos\xi} V - N_{22}\xi^p \frac{\sin\xi}{\cosh\eta-\cos\xi} U + N_{22}\xi^p A\sum_{m=1}^{N} a_{jm}^{\eta} V_{im} \tag{28}$$

$$T_{\xi\eta} = N_{13}\xi^p A\sum_{k=1}^{N} b_{jk}^{\eta} U_{ik} + N_{13}\xi^p A\sum_{l=1}^{N} a_{il}^{\xi} V_{lj} + N_{13}\xi^p \frac{\sin\xi}{\cosh\eta-\cos\xi} V + N_{13}\xi^p \frac{\sinh\eta}{\cosh\eta-\cos\xi} U \tag{29}$$

and coordinates of sampling points used in the *x* and *h* directions are defined respectively as:

$$\xi_i = R_i + \frac{R_o - R_i}{2}\left(1-\cos\left(\frac{i-1}{N-1}\right)\right), \quad i = 1,2,\ldots,N \tag{30}$$

$$\eta_j = 2\pi\left(\frac{j-1}{N}\right), \quad j = 1,2,\ldots,N \tag{31}$$

The differential quadrature discretized form of the equilibrium equations and boundary conditions can be expressed in matrix form as:

$$\begin{bmatrix} K_{bb} & K_{bd} \\ K_{db} & K_{dd} \end{bmatrix}\begin{Bmatrix} \Delta_b \\ \Delta_d \end{Bmatrix} = \begin{Bmatrix} f \\ 0 \end{Bmatrix} \tag{32}$$

where K represents the stiffness matrices and subscripts d and b represent domain and boundary points, respectively. Δ_d and Δ_b are, respectively, the displacement vector components (U, V) of the domain and boundary sampling points. By solving Eq. (32), an eigenvalue problem, one can obtain the displacement vectors at every grid point.

4. Results and Discussion

In order to present the results, consider a cylinder with the inner and outer boundaries at *x*=p/3 and *x*=p/4 respectively. Because the geometry of the considering problem with respect to both the X and Y axis is symmetric, only the first quarter of the considering geometry is solved to simplify the problem. Considering the material properties at the inner boundary are considered as: $N_{11}=94e9MPa$, $N_{12}=40.4e9MPa$, $N_{13}=53.8e9MPa$, $N_{22}=94e9MPa$. The inner boundary is subjected to hydrostatic pressure and the outer boundary is clamped along x and h directions:

$$\begin{aligned} &T_{\xi\xi}=10^6\,Pa && ,\text{at } \xi=\pi/3 \\ &T_{\xi\eta}=0 && ,\text{at } \xi=\pi/3 \\ &V(\xi,\eta)=U(\xi,\eta)=0 && ,\text{at } \xi=\pi/4 \end{aligned} \tag{33}$$

Figures 2, 3 and 4 show the tangled circles stresses along a line in a specific direction *h*= 0, 1, 2 for different material inhomogeneity respectively. From Fig. 2, it can be seen that initially the value of $T_{\xi\xi}$ decreases and then increases again from the inner boundary to the outer boundary respectively and this behavior is repeated for all inhomogeneity indexes. But the material index has little effect of stress in this direction. It can be seen from Fig. 3 that the $T_{\xi\xi}$ stress decreases from the inner to the outer boundary and the slop of the decrease is steeper near the inner boundary and gets more gradual near the outer boundary. It can be seen that the stress values have the same manner for all material inhomogeneity but at index p = -1 it has the minimum values of stress and the smoothest transition from inner to outer boundary. Figure 4 shows that the stress $T_{\xi\xi}$ decreases from the inner boundary to the outer boundary. Also, it can be seen in Figs. 2 and 4 that material inhomogeneity index changes don't make a noticeable change in $T_{\xi\xi}$ stress values along *h* = 0 and 2 directions so the changes with material inhomogeneity in midpoints have more values.

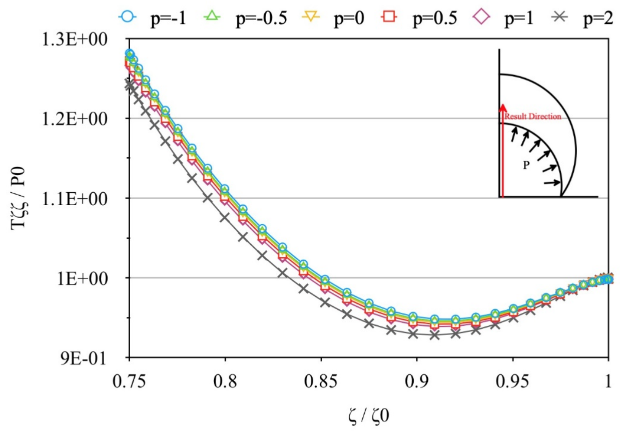

Fig. 2. $T_{\xi\xi}$ stress for the various material index at *h* = 0

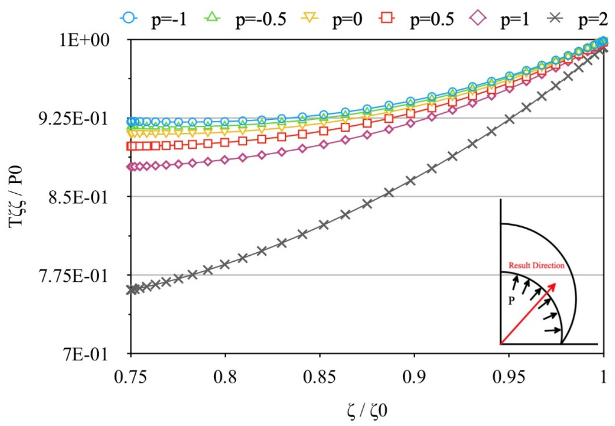

Fig. 3. $T_{\xi\xi}$ stress for the various material index at *h* = 1

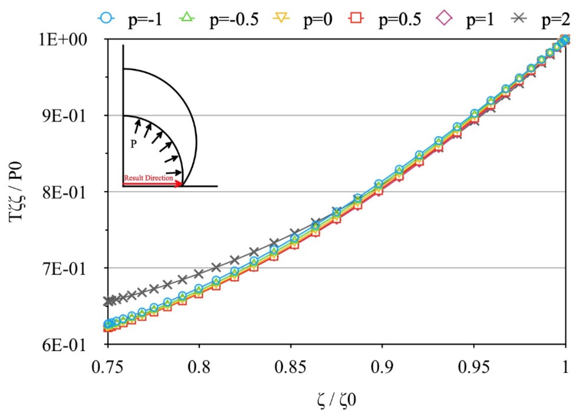

Fig. 4. $T_{\xi\xi}$ stress for the various material index at *h* = 2

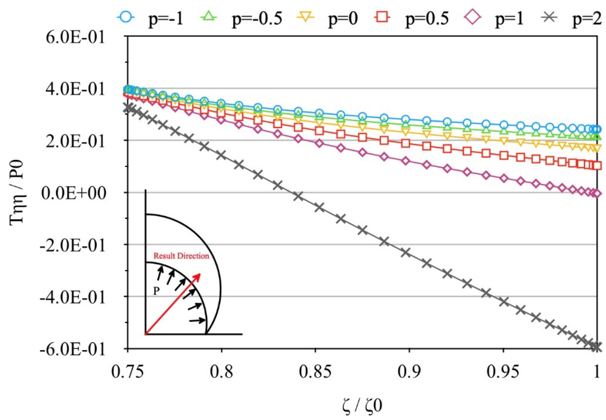

Fig. 5. $T_{\eta\eta}$ stress for the various material index at *h* = 0

Figures 5, 6 and 7 each show the $T_{\eta\eta}$ stress along a line in a specific direction *h* = 0, 1, 2 respectively for different material inhomogeneity. It can be seen that at *h* = 0 and 2 the effect of inhomogeneity index decreases from the inside boundary to outside so that it almost has no effect near the outside boundary. It can be seen in Fig. 6 that the $T_{\eta\eta}$ stress has the lowest stresses near the material inhomogeneity p = -1 and also changes in stress are smoother in comparison to other indexes.

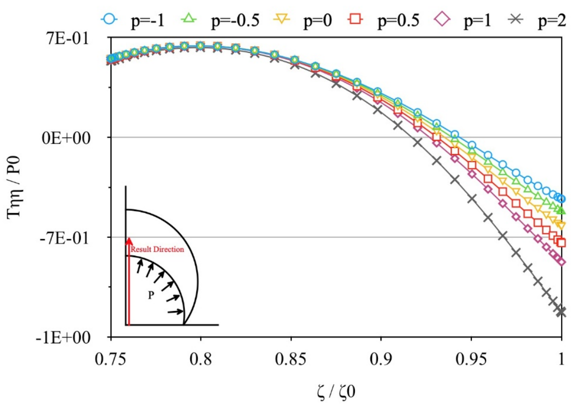

Fig. 6. $T_{\eta\eta}$ stress for the various material index at h = 1

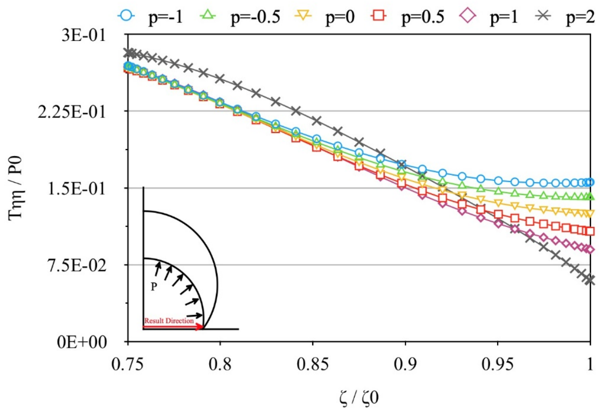

Fig. 7. $T_{\eta\eta}$ stress for the various material index at h = 2

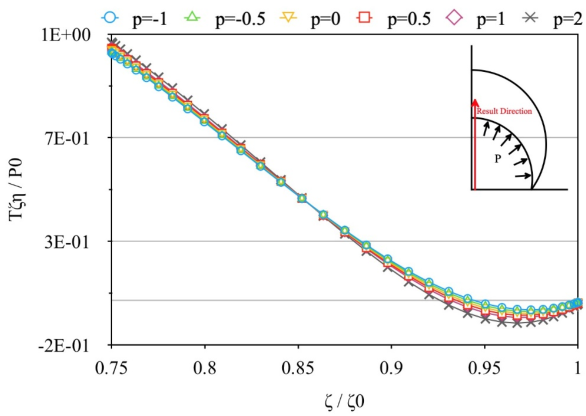

Fig. 8. $T_{\xi\eta}$ stress for the various material index at h = 0

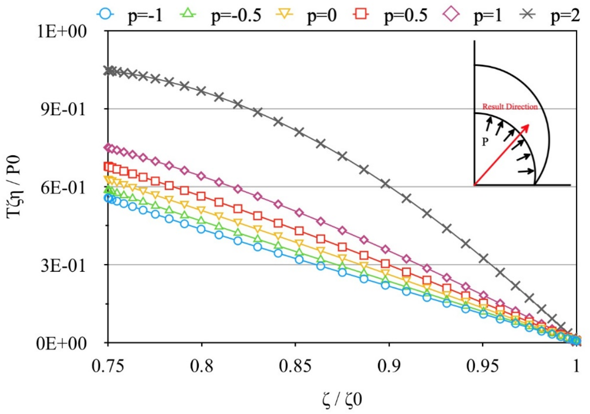

Fig. 9. $T_{\xi\eta}$ stress for the various material index at h = 1

Figures 8, 9 and 10 show the shear stress $T_{\xi\eta}$ along three considering direction h = 0, 1, 2 for various material inhomogeneity. Figure 8 shows the shear stress increases from the inner boundary to the outer boundary and the inhomogeneity index has little to no effect on the amount of stress. It can be seen in Fig. 9 that the stress raises almost linearly from the inner to outer boundary and has the lowest stress at index p = -1 and at h = 2 the slope of stress is steep near the inner boundary and the stress is rising then near the outer boundary it starts falling gradually. Also, it can be seen from Fig. 9 that the shear stress in midpoints changes linearly with material inhomogeneity.

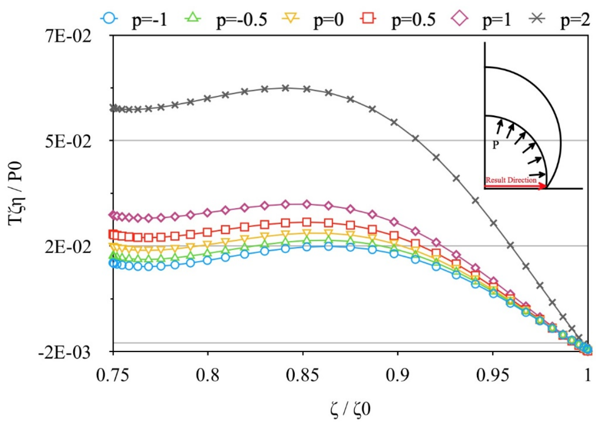

Fig. 10. $T_{\xi\eta}$ stress for the various material index at h = 2

To show the 3D stress in the thickness of considering geometry, Figs. 11 to 13 are presented. In these figures, the material inhomogeneity index considered as p=1. Figure 11 shows $T_{\xi\xi}$ stress through one-quarter of the geometry for p = 1. It can be seen that the boundary conditions considered in Eq. (15) are satisfied. Also, we can observe that in x = 1 we have the maximum stress as we can expect from the geometry. It is clear that the stress at the inner surface satisfies the boundary condition but the stress at the outer surface changes according to the shape of the geometry. Figures 12 show the $T_{\eta\eta}$ through the thickness of the geometry and it can be seen that at h = 0 the changes in stress is almost linear and gradually changed. But at higher values for h the changes in stress has more changes. Figure 13 shows the shear stress by considering geometry. We can see the increase in shear stress in both considering geometry directions because of the asymmetric geometry of the problem. Also, the boundary conditions are satisfied according to Eq. (15).

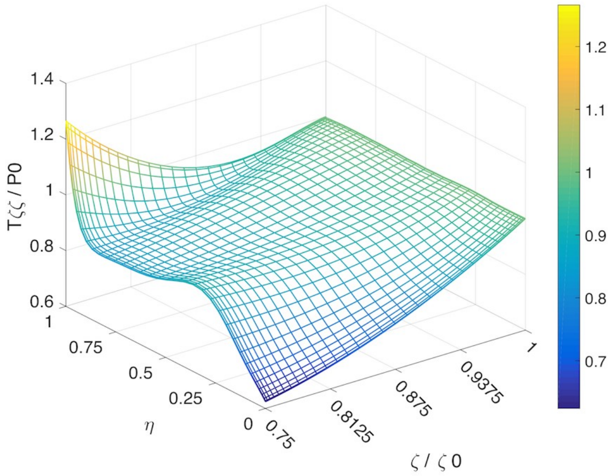

Fig. 11. $T_{\xi\xi}$ stress in the FGM geometry for p = 1

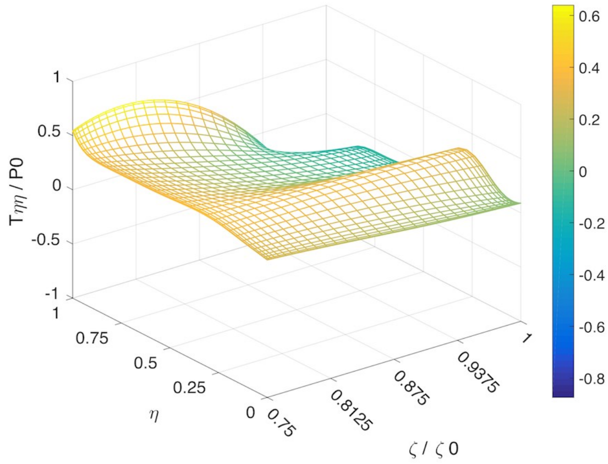

Fig. 12. $T_{\eta\eta}$ stress in the FGM geometry for p = 1

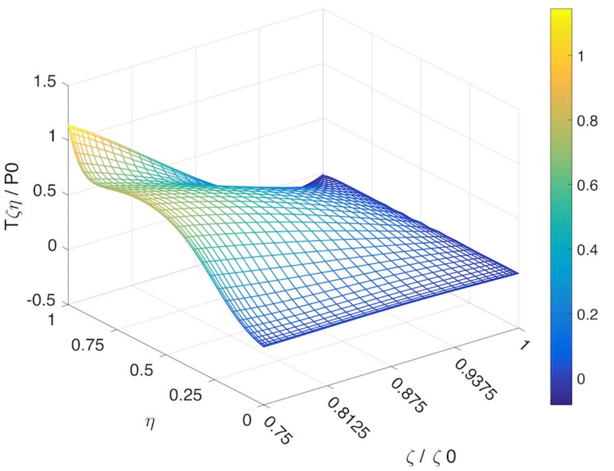

Fig. 13. Shear stress in the FGM geometry for p = 1

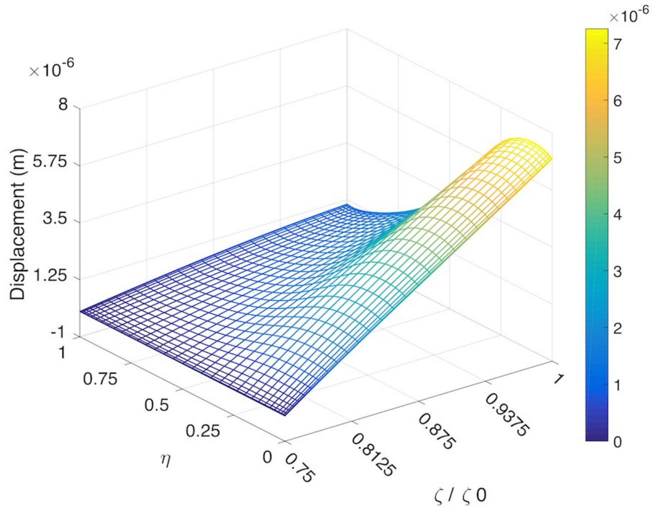

Fig. 14. x displacement in the FGM geometry for p = 1

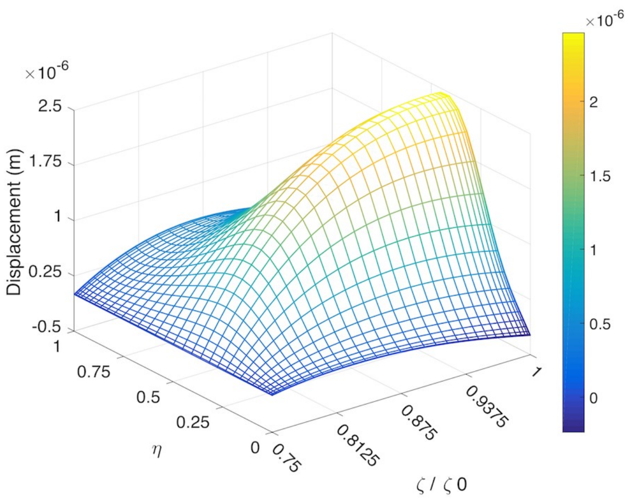

Fig. 15. h displacement in the FGM geometry for p = 1

Figures 14 and 15 present the displacements along x and h directions through the thickness of the geometry respectively.

According to the considered boundary conditions we can see that the displacements at the outer boundary in both figures lead to the value zero. Also, it can be seen that the x displacement has a maximum value it the middle of the inside of the geometry and it changes along x and h directions.

5. Validating of the Results

To validate the results, considering h = 0 and $\pi/6 \le \xi \le \pi/3$ for considering geometry at bipolar cylindrical coordinate. Using Eq. (A1), the geometry at this point, changes to a hollow cylinder with the inner and outer radius equal to R_i=1.73 and R_i=3.73 respectively. By considering these condition, the results can compare with reference [42]. For comparison purpose, we consider the material index m = 0.5 for the inhomogeneity. Figure 16 shows the stress $T_{\xi\xi}$ through the thickness to compare the results presented in this paper and the results reported in reference [42]. It can be seen that there is good agreement between the results.

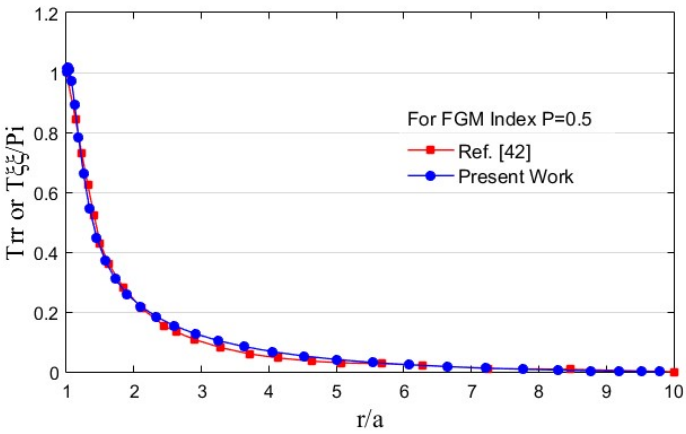

Fig. 16. Comparison of stress $T_{\xi\xi}$ between the present results and those of ref. [42] for a power law index p = 0.5

6. Conclusion

This paper presents a numerical solution for a real problem, functionally graded chamber of hydraulic gear pumps. Because of the complex considering geometry and similarity, a bipolar cylindrical coordinate system is considered for governing equations and boundary conditions. The material properties are varied along the two tangled circles with power-law function. By considering the problem, the governing equations lead to two coupled differential equations. To solve the governing equations, differential quadrature method is used. The results show that the material inhomogeneity and considering geometry can change the stress value efficiently. The results and presented method for extracting and solving the problem in this paper can be used for designing similar geometry more accurate. The results of this research are compared with those reported in the previous work.

Conflict of Interest

The author(s) declared no potential conflicts of interest with respect to the research, authorship and publication of this article.

Funding

The author(s) received no financial support for the research, authorship and publication of this article.

References

[1] Ersoy, H., Mercan K., Civalek O., Frequencies of FGM shells and annular plates by the methods of discrete singular convolution and differential quadrature methods, *Composite Structures*, 183, 2018, 7-20.
[2] Naderi Beni, N., Botshekanan Dehkordi M., An extension of Carrera unified formulation in polar coordinate for analysis of circular sandwich plate with FGM core using GDQ method, *Composite Structures*, 185, 2018, 421-434.
[3] Wang, X., Yuan Z., Accurate stress analysis of sandwich panels by the differential quadrature method, *Applied Mathematical Modelling*, 43, 2017, 548-565.
[4] Hosseini, M., Dini A., Eftekhari M., Strain gradient effects on the thermoelastic analysis of a functionally graded micro-rotating cylinder using generalized differential quadrature method, *Acta Mechanica*, 228(5), 2017, 1563-1580.
[5] Demirbas M.D., Thermal stress analysis of functionally graded plates with temperature-dependent material properties using theory of elasticity, *Composites Part B: Engineering*, 131, 2017, 100-124.

[6] Mehditabar, A., Rahimi G., Sadrabadi S.A., Three-dimensional magneto-thermo-elastic analysis of functionally graded cylindrical shell, *Applied Mathematics and Mechanics*, 38(4), 2017, 479-494.
[7] Brischetto, S., Tornabene f., Fantuzzi N., Viola E., 3D exact and 2D generalized differential quadrature models for free vibration analysis of functionally graded plates and cylinders, *Meccanica*, 51(9), 2016, 2059-2098.
[8] Aliyari Parand, A., Alibeigloo A., Static and vibration analysis of sandwich cylindrical shell with functionally graded core and viscoelastic interface using DQM, *Composites Part B: Engineering*, 126, 2017, 1-16.
[9] Adineh, M., Kadkhodayan M., Three-dimensional thermo-elastic analysis and dynamic response of a multi-directional functionally graded skew plate on elastic foundation, *Composites Part B: Engineering*, 125, 2017, 227-240.
[10] Jafari Fesharaki J., Jafari Fesharaki V., Yazdipoor M., Razavian B., Two-dimensional solution for electro-mechanical behavior of functionally graded piezoelectric hollow cylinder, *Applied Mathematical Modelling*, 36(11), 2012, 5521-5533.
[11] Shafiei, N., Mirjavadi S.S., Afshari B.M., Rabby S., Hamouda A. M. S., Nonlinear thermal buckling of axially functionally graded micro and nanobeams, *Composite Structures*, 168, 2017, 428-439.
[12] Zghal, S., Frikha A., Dammak F., Mechanical buckling analysis of functionally graded power-based and carbon nanotubes-reinforced composite plates and curved panels, *Composites Part B: Engineering*, 150, 2018, 165-183.
[13] Zghal, S., Frikha A., Dammak F., Free vibration analysis of carbon nanotube-reinforced functionally graded composite shell structures, *Applied Mathematical Modelling*, 53, 2018, 132-155.
[14] Yang J., Wu H., Kitipornchai S., Buckling and postbuckling of functionally graded multilayer graphene platelet-reinforced composite beams, *Composite Structures*, 161, 2017, 111-118.
[15] Daviran S., Sassan M., Alibakhsh K., Omid A., Differential quadrature method for thermal shock analysis of CNT reinforced metal-ceramic functionally graded disc, *Composite Structures*, 161, 2017, 299-307.
[16] Ansari R., Shojaei M.F., Gholami R., Size-dependent nonlinear mechanical behavior of third-order shear deformable functionally graded microbeams using the variational differential quadrature method, *Composite Structures*, 136, 2016, 669-683.
[17] Atrian, A., Jafari Fesharaki J., Nourbakhsh S.H., Thermo-electromechanical behavior of functionally graded piezoelectric hollow cylinder under non-axisymmetric loads, *Applied Mathematics and Mechanics*, 36(7), 2015, 939-954.
[18] Bahadori R., Najafizadeh M.M., Free vibration analysis of two-dimensional functionally graded axisymmetric cylindrical shell on Winkler–Pasternak elastic foundation by First-order Shear Deformation Theory and using Navier-differential quadrature solution methods, *Applied Mathematical Modelling*, 39(16), 2015, 4877-4894.
[19] Ansari R., Faghih Shojaei M., Shahabodini A., Bazdid-Vahdati M., Three-dimensional bending and vibration analysis of functionally graded nanoplates by a novel differential quadrature-based approach, *Composite Structures*, 131, 2015, 753-764.
[20] Zghal S., Frikha A., Dammak F., Static analysis of functionally graded carbon nanotube-reinforced plate and shell structures, *Composite Structures*, 176, 2017, 1107-1123.
[21] Frikha A., Zghal S., Dammak F., Dynamic analysis of functionally graded carbon nanotubes-reinforced plate and shell structures using a double directors finite shell element, *Aerospace Science and Technology*, 78, 2018, 438-451.
[22] Alibeigloo A., Nouri V., Static analysis of functionally graded cylindrical shell with piezoelectric layers using differential quadrature method, *Composite Structures*, 92(8), 2010, 1775-1785.
[23] Li D., Deng Z., Chen G., Xiao H., Zhu L., Thermomechanical bending analysis of sandwich plates with both functionally graded face sheets and functionally graded core, *Composite Structures*, 169, 2017, 29-41.
[24] Norouzi H., Alibeigloo A., Three dimensional static analysis of viscoelastic FGM cylindrical panel using state space differential quadrature method, *European Journal of Mechanics - A/Solids*, 61, 2017, 254-266.
[25] Civalek Ö., Free vibration of carbon nanotubes reinforced (CNTR) and functionally graded shells and plates based on FSDT via discrete singular convolution method, *Composites Part B: Engineering*, 111, 2017, 45-59.
[26] Akbari Alashti R., Khorsand M., Three-dimensional dynamo-thermo-elastic analysis of a functionally graded cylindrical shell with piezoelectric layers by DQ-FD coupled, *International Journal of Pressure Vessels and Piping*, 96, 2012, 49-67.
[27] Zghal S., Frikha A., Dammak F., Non-linear bending analysis of nanocomposites reinforced by graphene-nanotubes with finite shell element and membrane enhancement, *Engineering Structures*, 158, 2018, 95-109.
[28] Frikha A., Zghal S., Dammak F., Finite rotation three and four nodes shell elements for functionally graded carbon nanotubes-reinforced thin composite shells analysis, *Computer Methods in Applied Mechanics and Engineering*, 329, 2018, 289-311.
[29] Yas M.H., Sobhani Aragh B., Elasticity solution for free vibration analysis of four-parameter functionally graded fiber orientation cylindrical panels using differential quadrature method, *European Journal of Mechanics - A/Solids*, 30(5), 2011, 631-638.
[30] Shojaei M.F., Ansari R., Variational differential quadrature: a technique to simplify numerical analysis of structures, *Applied Mathematical Modelling*, 49, 2017, 705-738.
[31] Setoodeh, A.R., Tahani M., Selahi E., Hybrid layerwise-differential quadrature transient dynamic analysis of functionally graded axisymmetric cylindrical shells subjected to dynamic pressure, *Composite Structures*, 93(11), 2011, 2663-2670.
[32] Malekzadeh P., Three-dimensional thermal buckling analysis of functionally graded arbitrary straight-sided quadrilateral plates using differential quadrature method, *Composite Structures*, 93(4), 2011, 1246-1254.
[33] Jodaei A., Jalal M., Yas M.H., Free vibration analysis of functionally graded annular plates by state-space based differential quadrature method and comparative modeling by ANN, *Composites Part B: Engineering*, 43(2), 2012, 340-353.
[34] Janghorban M., Zare A., Free vibration analysis of functionally graded carbon nanotubes with variable thickness by differential quadrature method, *Physica E: Low-dimensional Systems and Nanostructures*, 43(9), 2011, 1602-1604.

[35] Alibeigloo A., Liew K., Elasticity solution of free vibration and bending behavior of functionally graded carbon nanotube-reinforced composite beam with thin piezoelectric layers using differential quadrature method, *International Journal of Applied Mechanics*, 7(01), 2015, 1550002.
[36] Trabelsi S., Frikha A., Zghal S., Dammak F., Thermal post-buckling analysis of functionally graded material structures using a modified FSDT, *International Journal of Mechanical Sciences*, 144, 2018, 74-89.
[37] Trabelsi S., Frikha A., Zghal S., Dammak F., A modified FSDT-based four nodes finite shell element for thermal buckling analysis of functionally graded plates and cylindrical shells, *Engineering Structures*, 178, 2019, 444-459.
[38] Heydarpour Y., Malekzadeh P., Golbahar Haghighi M., Vaghefi M., Thermoelastic analysis of rotating laminated functionally graded cylindrical shells using layerwise differential quadrature method, *Acta Mechanica*, 223(1), 2012, 81-93.
[39] Alashti R.A., Khorsand M., Three-dimensional thermo-elastic analysis of a functionally graded cylindrical shell with piezoelectric layers by differential quadrature method, *International Journal of Pressure Vessels and Piping*, 88(5), 2011, 167-180.
[40] Bellman R., Kashef B.G., Casti J., Differential quadrature: A technique for the rapid solution of nonlinear partial differential equations, *Journal of Computational Physics*, 10(1), 1972, 40-52.
[41] Shu C., Differential Quadrature and Its Application in Engineering. 2000, London: Springer-Verla.
[42] Horgan C.O., Chan A.M., The Pressurized Hollow Cylinder or Disk Problem for Functionally Graded Isotropic Linearly Elastic Materials, *Journal of Elasticity*, 55(1), 1999, 43-59.
[43] Heinbockel J.H., *Introduction to Tensor Calculus and Continuum Mechanics*. 2001: Trafford.

Appendix A

The relation between Cartesian and bipolar cylindrical coordinate is presented as [43]:

$$\begin{aligned} x &= \frac{a\sinh\eta}{\cosh\eta-\cos\xi} && 0\le\xi\le 2\pi && h_1 = h_2 \\ y &= \frac{a\sin\xi}{\cosh\eta-\cos\xi} && -\infty\le\eta\le\infty && h_2 = \frac{a}{\cosh\eta-\cos\xi} \\ z &= z && -\infty\le z\le\infty && h_3 = 1 \end{aligned} \tag{A1}$$

and by the intersection of the coordinates, the coordinate curves take the form:

$$\begin{aligned} &(x-a\coth\eta)^2+y^2=\frac{a^2}{\sinh^2\eta} && \text{cylinder} \\ &x^2+(y-a\cot\xi)^2=\frac{a^2}{\sin^2\xi} && \text{cylinder} \\ &z=cons. \end{aligned} \tag{A2}$$

So, the position vector for each point is:

$$\vec{r}=\frac{a\sinh\eta}{\cosh\eta-\cos\xi}\vec{i}+\frac{a\sin\xi}{\cosh\eta-\cos\xi}\vec{j}+z\vec{k} \tag{A3}$$

and the unit vector for each direction yields:

$$\begin{aligned} \hat{e}_\xi &= \frac{1}{h_1}e_\xi=\frac{-\sinh\eta\sin\xi}{\cosh\eta-\cos\xi}\vec{i}+\frac{\cos\xi\cosh\eta-1}{\cosh\eta-\cos\xi}\vec{j} \\ \hat{e}_\eta &= \frac{1}{h_2}e_\eta=\frac{1-\cosh\eta\cos\xi}{\cosh\eta-\cos\xi}\vec{i}+\frac{-\sin\xi\sin\eta}{\cosh\eta-\cos\xi}\vec{j} \\ \hat{e}_z &= \frac{1}{h_3}e_z=\vec{k} \end{aligned} \tag{A4}$$

Consider the displacement vector in the bipolar cylindrical coordinate as:

$$\vec{u}=u\hat{e}_\xi+v\hat{e}_\eta+w\hat{e}_z \tag{A5}$$

Also, the strain tensor takes the form:

$$\varepsilon=\frac{1}{2}(\nabla u+\nabla u^T) \tag{A6}$$

Substituting Eq. (A5) into (A6) and using Eqs. (A1)-(A4), the strains in the bipolar cylindrical coordinate system are

$$\varepsilon_{\xi\xi} = \frac{(\cosh\eta - \cos\xi)}{a}\frac{\partial u}{\partial \xi} - \frac{\sinh\eta}{a}v$$
$$\varepsilon_{\eta\eta} = -\frac{\sin\xi}{a}u + \frac{(\cosh\eta - \cos\xi)}{a}\frac{\partial v}{\partial \eta} \tag{A7}$$
$$\varepsilon_{\xi\eta} = \frac{1}{2}(\frac{(\cosh\eta - \cos\xi)}{a}\frac{\partial u}{\partial \eta} + \frac{(\cosh\eta - \cos\xi)}{a}\frac{\partial v}{\partial \xi} + \frac{\sin\xi}{a}v + \frac{\sinh\eta}{a}u)$$

Appendix B

The static equilibrium equation in a linear elastic material can be given by

$$T^i_{i,j} + \rho b_i = 0 \qquad i, j = 1,2,3 \tag{B1}$$

where $T^i_{i,j}$ is the stress tensor, r is the density, and b_i is the external body forces per unit mass. Assuming an orthogonal coordinate system, the stress tensor can be expressed as [43]:

$$T^i_{i,j} = \frac{1}{\sqrt{g}}\frac{\partial}{\partial x^j}(\sqrt{g}T^j_i) - [ij,m]T^{mj} \tag{B2}$$

where "g" is the metric components of the orthogonal system and can be expressed as:

$$g_{ij} = \begin{pmatrix} h_1^2 & 0 & 0 \\ 0 & h_2^2 & 0 \\ 0 & 0 & h_3^2 \end{pmatrix} \tag{B3}$$

and the equilibrium equations in terms of physical components are expressed as:

$$\Sigma_{j=1}^{3}\frac{1}{\sqrt{g}}\frac{\partial}{\partial x^j}(\frac{\sqrt{g}h_i T_{ij}}{h_j}) - \frac{1}{2}\Sigma_{j=1}^{3}\frac{T_{jj}}{h_j^2}\frac{\partial(h_j^2)}{\partial x^i} + h_i\rho b_i = 0 \tag{B4}$$

where there is no summation on "i". Using equations (A1) and (B1)-(B4), the equilibrium equation irrespective of the body force along the "x" and "h" directions yields

$$\frac{\partial T_{\xi\xi}}{\partial \xi} + \frac{\partial T_{\xi\eta}}{\partial \eta} + \frac{\sin\xi}{(\cosh\eta - \cos\xi)}(T_{\eta\eta} - T_{\xi\xi}) = 0$$
$$\frac{\partial T_{\eta\eta}}{\partial \eta} + \frac{\partial T_{\xi\eta}}{\partial \xi} + \frac{2\sin\xi}{(\cosh\eta - \cos\xi)}T_{\xi\eta} + \frac{\sinh\eta}{(\cosh\eta - \cos\xi)}(T_{\xi\xi} - T_{\eta\eta}) = 0 \tag{B5}$$

Appendix C

The material property constants for equations (6) and (7) are

$$c_1 = \frac{N_{13}}{N_{11}},\quad c_2 = \frac{N_{13} - N_{12}}{N_{11}},\quad c_3 = \frac{N_{13} - N_{11}}{N_{11}},\quad c_4 = \frac{N_{22} + N_{13}}{N_{11}},\quad c_5 = \frac{-2N_{12}}{N_{11}},\quad c_6 = \frac{2N_{13}}{N_{11}}$$
$$c_7 = \frac{N_{12} - N_{22}}{N_{11}},\quad c_8 = -1,\quad c_9 = \frac{N_{11} - N_{12}}{N_{11}},\quad c_{10} = \frac{N_{13}}{N_{22}},\quad c_{11} = \frac{N_{12} + N_{13}}{N_{22}},\quad c_{12} = \frac{2N_{22} - 2N_{12}}{N_{22}}$$
$$c_{13} = \frac{N_{13}}{N_{22}},\quad c_{14} = \frac{2N_{12} + N_{13} + N_{11}}{N_{22}},\quad c_{15} = \frac{-N_{22} - N_{13}}{N_{22}},\quad c_{16} = \frac{-N_{11} - N_{12}}{N_{22}},\quad c_{17} = \frac{-2N_{13}}{N_{22}} \tag{C1}$$
$$c_{18} = \frac{-N_{12}}{N_{22}},\quad c_{19} = \frac{-N_{22} - N_{12} - 2N_{13}}{N_{22}}$$